Received: 12 December 2022 | Revised: 10 March 2023 | Accepted: 11 March 2023
DOI: 10.1002/rcm.9508

RESEARCH ARTICLE

Rapid Communications in Mass Spectrometry WILEY

Matrix-independent boron isotope analysis of silicate and carbonate reference materials by ultraviolet femtosecond laser ablation multi-collector inductively coupled plasma mass spectrometry with application to the cold-water coral *Desmophyllum dianthus*

Grit Steinhoefel[1] | Kristina K. Beck[1,2,3] | Albert Benthien[1] | Klaus-Uwe Richter[1] | Gertraud M. Schmidt-Grieb[1] | Jelle Bijma[1]

[1]Helmholtz-Zentrum für Polar- und Meeresforschung, Alfred-Wegener-Institut, Bremerhaven, Germany
[2]Universität Bremen, Bremen, Germany
[3]University of Edinburgh, Edinburgh, UK

Correspondence
G. Steinhoefel, Alfred-Wegener-Institut, Helmholtz-Zentrum für Polar- und Meeresforschung, Am Handelshafen 12, 27570 Bremerhaven, Germany.
Email: grit.steinhoefel@awi.de

Present address
Kristina K. Beck, University of Edinburgh, Edinburgh, UK.

Funding information
AWI Strategy Fund, Grant/Award Number: Project DACCOR; Bundesministerium für Bildung und Forschung, Grant/Award Numbers: 01DN15024, 20140041

Rationale: Boron isotopes are a powerful tool for pH reconstruction in marine carbonates and as a tracer for fluid–mineral interaction in geochemistry. Microanalytical approaches based on laser ablation multi-collector inductively coupled plasma mass spectrometry (LA-MC-ICP-MS) often suffer from effects induced by the sample matrix. In this study, we investigate matrix-independent analyses of B isotopic ratios and apply this technique to cold-water corals.

Methods: We employ a customized 193 nm femtosecond laser ablation system (Solstice, Spectra-Physics) coupled to a MC-ICP-MS system (Nu Plasma II, Nu Instruments) equipped with electron multipliers for *in situ* measurements of B isotopic ratios ($^{11}B/^{10}B$) at the micrometric scale. We analyzed various reference materials of silicate and carbonate matrices using non-matrix matched calibration without employing any correction. This approach was then applied to investigate defined increments in coral samples from a Chilean fjord.

Results: We obtained accurate B isotopic ratios with a reproducibility of ±0.9‰ (2 SD) for various reference materials including silicate glasses (GOR132-G, StHs6/80-G, ATHO-G and NIST SRM 612), clay (IAEA-B-8) and carbonate (JCp-1) using the silicate glass NIST SRM 610 as calibration standard, which shows that neither laser-induced nor ICP-related matrix effects are detectable. The application to cold-water corals (*Desmophyllum dianthus*) reveals minor intra-skeleton variations in $\delta^{11}B$ with average values between 23.01‰ and 25.86‰.

Conclusions: Our instrumental set-up provides accurate and precise B isotopic ratios independently of the sample matrix at the micrometric scale. This approach opens a wide field of application in geochemistry, including pH reconstruction in biogenic carbonates and deciphering processes related to fluid–mineral interaction.

1 | INTRODUCTION

Fractionation of B isotopes (expressed as $\delta^{11}B$) has emerged as powerful tool in both low- and high-temperature geochemistry. Examples include paleo-oceanography as a pH proxy, biomineralization, cosmochemistry and fluid–mineral interactions such as in hydrothermal system, subduction zones and in weathering environments.[1] The investigation of the B isotopic composition in marine biogenic carbonates (e.g., foraminifera, corals, coralline algae, brachiopods) has received especially large interest as it provides a unique opportunity to reconstruct seawater pH and atmospheric pCO_2 concentrations over geological time scales.[2–7]

Boron isotopic analyses of bulk samples using multi-collector inductively coupled plasma mass spectrometry (MC-ICP-MS) or thermal ionization mass spectrometry (TIMS) are now routinely performed in many laboratories.[8,9] These analytical approaches provide accurate and highly precise B isotopic ratios (better than 0.5‰, 2 SD) but spatial resolution is limited and careful separation of B is often required prior to analysis. Microanalytical *in situ* approaches using secondary ion mass spectrometry (SIMS) or laser ablation (LA) MC-ICP-MS are more challenging because of low signal intensities, effects related to the sample matrix and the requirement of appropriate homogeneous reference materials. However, they offer the potential to decipher processes at the micrometric scale and enhance temporal resolution for instance for reconstructing paleo seawater pH.[10,11] Analyses by both SIMS and LA-MC-ICP-MS (nanosecond (ns) and femtosecond (fs) LA) demand little sample preparation and consume small amounts of sample material (<1 ng of B), but may involve matrix-matched calibration or correction modes.[6,11–18] Obtained data have higher uncertainties compared to bulk solution analysis due to natural small-scale heterogeneity in $\delta^{11}B$ within the sample, higher analytical uncertainties and potential heterogeneities of calibration standards, which may limit applications especially in paleo-oceanography.[11]

In particular, approaches based on LA coupled to a MC-ICP-MS instrument have received increasing interest in recent years. However, matrix effects may result in low accuracy or low precision, especially when sample material and calibration standard differ in matrix composition. Laser-related matrix effects either occur at the ablation site if the ablation process produces non-stoichiometric aerosol or are linked to particle-size-related fractionation, that is, large particles, which might be affected by less efficient transport or incomplete ionization in the plasma of the mass spectrometer. These effects have been commonly observed for ns LA systems, whereas both are largely absent when employing fs pulses (1 fs = 10^{-15} s).[19–23] Another source of matrix effects refers to processes within the ICP-MS including plasma load effects, instrumental mass discrimination and interferences, which might become relevant for both ns and fs LA.[24] While most studies focused on biogenic carbonates,[11,13,14,18,25–27] some silicates have also been analyzed, however with a focus on materials with high B content (e.g., tourmaline) with reported precisions ranging between 0.5‰ and 2‰ (2 SD).[12,16,23,28–33] Matrix-independent calibration is feasible but numerous analytical protocols include a correction mode to compensate for matrix-induced biases to obtain accurate $\delta^{11}B$ values,[12,18,26] while other authors have not observed such an offset.[11,13,14,23,27,30] Observed offsets in $\delta^{11}B$ correlate with B/Ca ratios for carbonate matrices, which was interpreted as an unresolved interference on masses of B isotopes due to scattered Ca ions when using a Thermo Neptune Plus MC-ICP-MS.[18,26] More recently, another study[12] built upon these findings and explored this matrix-induced interference for silicate matrices of mafic rock compositions using a similar instrumental set-up and improved the methodology to correct for the observed bias in $\delta^{11}B$. Interestingly, this interference by scattered Ca ions has not been observed for carbonate using a Nu Plasma II MC-ICP-MS (Nu Instruments) coupled to a UV fs LA system[11] making non-matrix matched calibration feasible without corrections.

In the study reported here, we explored the capability of this instrumental set-up for *in situ* B isotope analysis for various reference materials covering carbonate and silicate matrices using the NIST SRM 610 glass as calibration standard and applied this technique to the cold-water coral *Desmophyllum dianthus* from the Chilean fjord region (Comau Fjord). We demonstrate that this set-up provides accurate and precise B isotopic data independent of the sample matrix. This approach provides an attractive tool to enhance the application of B isotopes in biogenic carbonates and as a tracer for fluid–mineral interaction in high- and low-temperature environments at the micrometric scale.

2 | EXPERIMENTAL

2.1 | Reference materials

We chose reference materials to cover various sample matrices and B contents, including carbonate, clay and silicates from rhyolitic to komatiitic composition to explore matrix-independency for B isotope analysis using UV fs LA coupled to a Nu Plasma II MC-ICP-MS (Table 1). This selection covers a range in B content relative to major matrix elements like Ca and Si, which can affect accuracy.[12,18,26] The investigated reference materials comprise JCp-1 (coral-carbonate powder; [B] = 47 ppm), IAEA-B-8 (clay powder; [B] = 100 ppm), NIST SRM 612 (silicate glass; [B] = 33 ppm) and the silicate reference glass series “MPI-DING”: ATHO-G (rhyolite; [B] = 6 ppm), StHs6/80-G (andesite; [B] = 11 ppm) and GOR132-G (komatiites; [B] = 18 ppm). Powdered reference materials were pressed into powder pellets using a hydraulic press, whereas glass standards were embedded in epoxy resin and polished as described in more detail elsewhere.[34,35]

2.2 | Cold-water coral samples

The investigated cold-water coral samples of *D. dianthus* are part of a sample collection from a field experiment conducted in the Comau Fjord (September 2016 to July 2017), which is located in the northern part of the Chilean fjord region.[37] *D. dianthus* is a solitary azooxanthellate deep-sea cold-water coral and is the most abundant coral species in this fjord, occurring from 20 m down to the maximum

TABLE 1 Determined B isotopic composition ($\delta^{11}B$) of reference materials by UV fs LA-MC-ICP-MS.

Reference material		$[B]^{a}$ ($\mu g\ g^{-1}$)	Rep. rate (Hz)	Signal ^{11}B (cps)	$\delta^{11}B$ (‰)	2 SD	*n*
JCp-1	Coral powder	48	10–20	220000	24.09	0.87	17
IAEA-B-8	Clay powder	100	5–10	320000	−5.82	0.67	11
NIST SRM 612	Silicate glass	35	125	200000	−0.49	0.65	14
GOR132-G	Komatiite glass	17	200	200000	8.34	1.10	9
StHs6/80-G	Andesite glass	11	250	200000	−4.24	0.62	5
ATHO-G	Rhyolite glass	6	250	110000	−4.22	0.54	3

[a]Preferred values as provided by the database *GeoReM*.[36]

TABLE 2 Seawater parameters and carbonate system calculated using CO2sys by Pierrot et al.[41]

Seawater pH_T	Temperature (°C)	Salinity (PSU)	Total alkalinity ($\mu mol\ kg^{-1}$)	DIC ($\mu mol\ kg^{-1}$)	Ω_{arag}	$[CO_3^{2-}]$ ($\mu mol\ kg^{-1}$)	pK_B	$\delta^{11}B_{borate}$ (‰)	$\delta^{11}B_{SW}$ (‰)	2 SD	*n*
Station A – fjord head (coral: BsCpI1-A)											
7.59	12.04 ± 0.78	32.17	2107	2078	0.75	49.20	8.76	14.51	40.37	0.15	3
Station F – fjord mouth (corals: CsCpI9-F, CsCpI4-F)											
7.86	12.31 ± 0.84	32.57	2181	2069	1.38	90.07	8.76	15.63	40.19	0.37	3

Seawater parameters were originally published in Beck et al[37] except for pK_B, $\delta^{11}B_{borate}$ and $\delta^{11}B_{SW}$. All data refer to January 2017, except for temperature data, which integrate over the time period from August 2016 to January 2017.

depth of the fjord at 480 m.[38] At 20 m water depth, the fjord exhibits a pH gradient from 7.6 to 7.9 with increasing values toward the mouth of the fjord in austral spring.[37,39] The mean spring water temperature is 12.2°C for shallow water, where it fluctuates frequently.[37] The investigated coral samples were collected at station A (42°26′38.64″ S, 72°25′8.46″ W) at the head of the fjord (sample BsCpI1-A) and at station F (42°09′46.20″ S, 72°35′47.28″ W) close to the mouth of the fjord (samples CsCpI4-F and CsCpI9-F). Station A is exposed to a higher terrigenous influence due to stream water inflow, whereas station F shows close to open-ocean conditions.

The coral samples were collected from the rock wall at shallow depth (about 20 m depth) by SCUBA divers in September 2016, stained with fluorescent calcein and re-deployed on plastic racks close to their original site. They were harvested about 4 months later in January 2017 to investigate the skeletal increment during austral spring, which marks a time period of high productivity in the fjord.[40] Salinity, dissolved oxygen concentration, seawater pH_T, water temperature, total alkalinity (TA) and dissolved inorganic carbon (DIC) were monitored by discrete water sampling and CTD casts at each investigated field site, whereas the aragonite saturation (Ω_{arag}) was calculated from TA and DIC using Microsoft Excel program CO2sys.[41] These data were obtained when corals were harvested in January 2017 but not at the beginning of the experiment in September 2016. However, data obtained almost a year later in August 2017 show very similar conditions in the fjord. The complete data set is published in Beck et al[37] and summarized in Table 2. All further work was conducted at the laboratories of the Alfred-Wegener-Institute in Bremerhaven. Coral samples were bleached twice with 6% hypochlorite solution to remove organic tissue, cleaned with Milli-Q water and dried before embedding in epoxy resin. We cut the embedded coral samples perpendicular to the growth axis at the upper part of the calyx (Figure 1). Prepared thick sections were polished and afterwards cleaned by ultrasonication in Milli-Q water. Prior to analysis by LA, we investigated the prepared samples by fluorescence microscopy (Axiovert 200 m, Zeiss, Germany) to visualize the fluorescent calcein staining line and to map skeletal increments (Figure 1C). Investigated increments of coral samples in prepared thick sections were similar in size. In addition, we sampled fjord water at stations A and F in January 2017 to measure the B isotopic composition of ambient seawater. Water samples were filtered through polycarbonate membrane filters (0.2 μm pore size), acidified with HNO_3 of ultrapure grade and stored in acid-clean polyethylene bottles at 4°C until analysis.

2.3 | Boron isotope analysis by UV fs LA coupled to MC-ICP-MS

2.3.1 | UV fs LA system

The customized UV fs LA system (Figure 2) is based on a Ti–sapphire regenerative amplifier system (Solstice, Spectra-Physics, USA) operating at a fundamental wavelength of 775 nm with a pulse width of 100 fs and pulse energy of 3.5 mJ $pulse^{-1}$. Consecutive harmonic generations using β-BaB_2O_4 crystals convert the beam subsequently into wavelengths of 356 nm at the second, 266 nm at the third and finally 193 nm at the fourth stage with a maximal output energy of 0.08 mJ $pulse^{-1}$. The repetition rate can be adjusted from 2 to 1000 Hz. The laser beam is then steered by four dichroic mirrors to a fully software-controlled microscope (Zeiss Axio Scope A1) equipped with several objectives with different magnifications (5-, 8- and 20-fold magnification), a charge-coupled device (CCD) camera for visualization and a motorized *x*, *y*, *z* sample stage designed by Rapp Opto Electronics. The beam is focused onto the sample surface using the eightfold

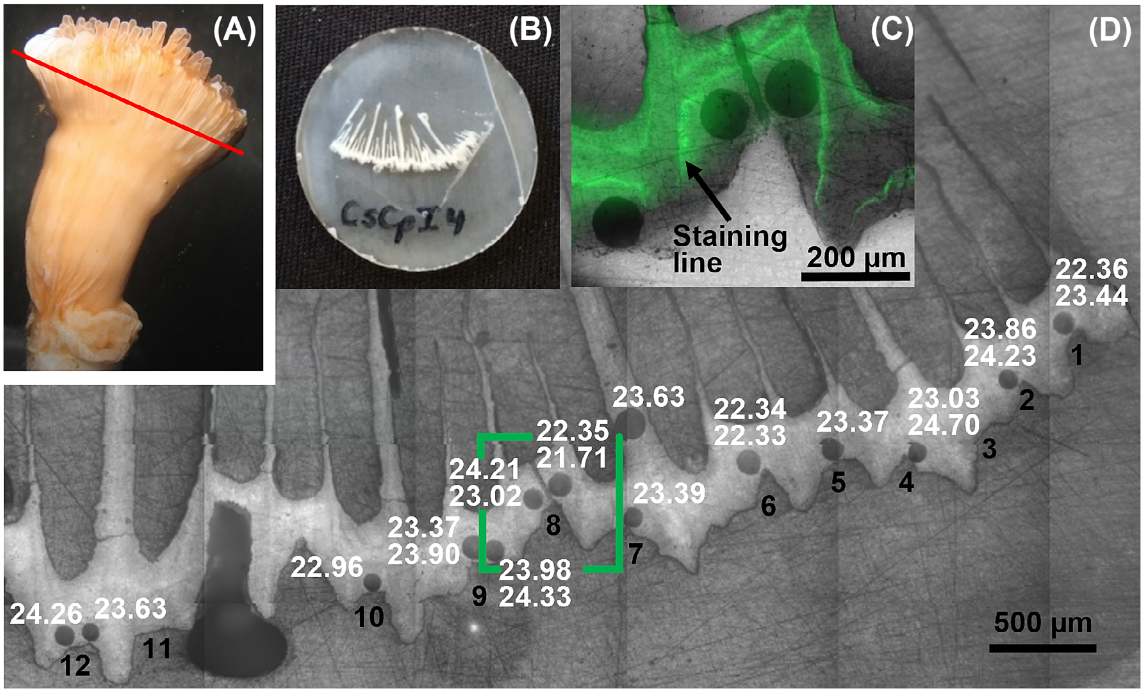

FIGURE 1 Analyses of B isotopic ratios at high spatial resolution of cold-water coral sample CsCpI4-F (*Desmophyllum dianthus*) from the Chilean Comau Fjord. (A) Example of *D. dianthus* (about 5 cm in height) with indicated cutting orientation for preparation of thick sections of coral skeletons. (B) Polished thick section (1 in. in diameter) with transversal section of coral sample CsCp I4-F prepared for LA analysis. (C) Detailed section of (D) (green inlet) taken by fluorescence microscopy. Boron isotope analyses were conducted using the helix mode of the LA system to cover circular areas (black spots) between the green fluorescent staining line and the outer edge of the skeleton, corresponding to the increment of austral summer. (D) Composite picture of the thick section of sample CsCp I4-F taken by reflected-light microscopy of the LA system. Numbered spots are ablated areas. Black numbers label the sample locations between septa (data from location 2 are not included in Table 4 because ablated area overlaps with staining line), whereas white numbers refer to measured $\delta^{11}B$ values given in permil (‰) for each spot. Some spots were analyzed twice. Boron isotopic ratios show minor variation, which appears to be randomly distributed. [Color figure can be viewed at wileyonlinelibrary.com]

objective, which is contemporaneously used for reflecting microscopy. The spot size can be adjusted between 2 and 50 µm by a motorized blend with apertures of various diameters. The sample cell is made of anti-static Teflon with an active volume of 45.2 cm^3 and closed with a lid with an integrated fused silica window with anti-reflection coating. The cell is flushed with He as carrier gas (*ca* 0.4 L min^{-1}), which is mixed with an Ar gas flow (*ca* 1.0 L min^{-1}) after the cell. The laser-produced aerosol is then transported via a Teflon tube to a Nu Plasma II MC-ICP-MS (Nu Instruments) for isotope analysis.

2.3.2 | Analysis of B isotopic ratios

In situ measurements of B isotopic ratios were performed using the UV fs LA system connected to a MC-ICP-MS (Nu Plasma II) at the AWI ICP facility of the Alfred-Wegener Institute, Bremerhaven, Germany. Details of the operation conditions are given in Table 3. Boron isotopic analyses were performed at low mass resolution of the mass spectrometer of about 2000, which is here defined as $m/\Delta m$, where m is the mass of the ion of interest and Δm is the mass difference between its 5% and 95% peak heights. This mass resolution is sufficient to resolve all molecular interferences as fourfold charged Ar and Ca or double charged Ne on ^{10}B to background levels for this set-up.[11] We employed sample and skimmer cones made of Ni for dry plasma conditions. The stable isotopes of B, ^{10}B and ^{11}B, were detected simultaneously on electron multiplier detectors at the positions IC0 and IC5, respectively, of the user-specific detector array of the MC-ICP-MS. The full-size electron multiplier detectors are capable of detecting very small signal intensities from a few hundred counts per second (cps) up to 2×10^6 cps, whereas its best stability for signal intensities is reached well below 10^6 cps. At the beginning of each analytical session, we measured B isotopic ratios for NIST SRM 610 at different signal intensities and adapted the deadtime of the detectors with the aim of measuring equal isotopic ratios independently of the signal intensity. A slight change on a daily base is likely induced by a drift of electronic gain of the detectors rather than the deadtime itself.[42,43] We used the standard-sampling-bracketing method and applied signal matching between bracketing standard and sample within 10% to correct for the instrumental mass bias and drift and to account for gain drift and imprecision of deadtime correction of the detectors. Tuning of the mass spectrometer aimed to optimize signal intensity and stability.

The NIST SRM 610 glass standard was used as bracketing standard for all investigated reference and sample materials. Laser repetition rates of 5 to 15 Hz resulted in signal intensities between 250 000 and 600 000 cps for ^{11}B for the bracketing standard NIST

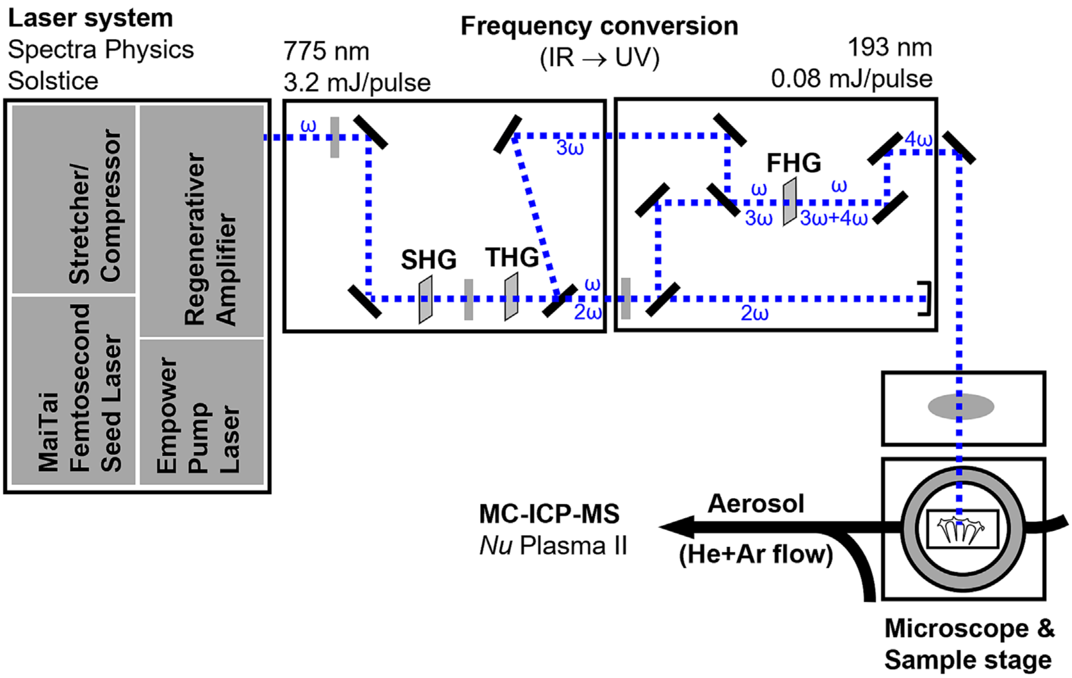

FIGURE 2 Schematic set-up of the UV fs LA system at the Alfred-Wegener-Institute in Bremerhaven. The set-up consists of a fs laser system (Solstice, Spectra Physics, USA), a unit which converts the laser beam from the IR into the UV range: gray rectangles are wave plates turning the laser beam by an angle of 90°; black rectangles are mirrors with wavelength-specific coatings; gray diamonds represent β-BaB_2O_4 crystals producing from the fundamental wavelength $\omega = 775$ nm consecutively the second, third and fourth harmonic generation (SHG, THG and FHG) with wavelengths of $2\omega = 356$ nm, $3\omega = 266$ nm and $4\omega = 193$ nm, respectively; and a microscope unit (Zeiss) with an integrated CCD camera and motorized sample stage, which is software controlled. [Color figure can be viewed at wileyonlinelibrary.com]

TABLE 3 Operation conditions of the UV fs LA system coupled to MC-ICP-MS.

UV fs LA system (based on Solstice, Spectra-Physics)	
Wavelength (nm)	193
Pulse width (fs)	~200
Pulse energy (J cm^{-2})	2
Spot diameter (μm)	35–50
Scan mode	Helix, scan speed of 2 mm s^{-1}
Repetition rate (Hz)	5–250
MC-ICP-MS (Nu Plasma II, Nu Instruments)	
Cool gas (L min^{-1})	13.0
Auxiliary gas (L min^{-1})	0.80
Sample gas Ar (L min^{-1})	0.90–1.02
Mixed gas He (L min^{-1})	0.38–0.44
RF power (W)	1300
Cones	Ni sample/skimmer cone for dry plasma conditions

SRM 610 ([B] = 351 μg g^{-1}). Depending on the sample material, the laser repetition rate was adjusted from 5 to 250 Hz to achieve signal matching with less than 10% deviation to the bracketing standard. The bracketing standard and sample materials (including coral samples) were analyzed using the helix-mode scan of the LA system, which was operated with a speed of 2 mm s^{-1} and a laser spot size of 40 μm in diameter to ablate a circular area with a diameter ranging between 100 and 200 μm.

Boron isotopic ratios of each reference material were obtained in one to five analytical sessions. Coral samples were analyzed as follows. Based on microscopic investigations, we selected suitable increments for LA analysis for each prepared coral sample. We analyzed increments between septa by avoiding the septa themselves and centers of calcification as both structures are known to show geochemical signatures[6,17,44,45] deviating from those recorded in the bulk skeleton. A single analysis was conducted at a large septum for comparison. For each analysis, the ablated area was adapted in size covering most of the increment to reveal a representative B isotopic ratio for the marked growth period of 4 months (Figure 1) rather than fine-scale variations due to heterogeneous calcification as mapped for some coral species.[10,46] Prior to each analysis, we pre-ablated the surface of the sample and standard material to remove potential surface contaminations. Boron isotopic ratios were acquired by measuring 150 cycles on the mass spectrometer with an integration time of 1 s. Such a short integration time allows detection of potential sample inhomogeneity or contamination, which can be accounted for in data evaluation. On-peak gas blank measurements for 30 cycles were performed prior to each analysis and subtracted from the signal intensities. Gas blanks reveal 2000 to 10 000 cps for ^{11}B and contribute less than 3% to the signal intensities obtained for reference and sample materials. Raw ratios of $^{11}B/^{10}B$ obtained for gas blanks are typically around 4.5, whereas those of sample materials range between 4.7 and 5.1. Therefore, background signals have minor effect and typical blank-corrected $\delta^{11}B$ values differ less than 0.5‰ from uncorrected values. Considering ablated volume and B content, a single analysis consumes sample material corresponding to less than 0.1 ng of B.

Data evaluation was performed using a self-created Microsoft Excel spreadsheet macro.[11] For each analysis, it subtracts the average blank measurements from signal intensities prior to the calculation of isotopic ratio for each cycle followed by an outlier test based on the deviation from the mean at the 95% confidence level. The resulting mean isotopic ratios and standard errors of bracketing standard and sample analyses were used for calculating $\delta^{11}B$ values and for performing error propagation. Reference materials were analyzed multiple times to explore accuracy and uncertainty for each sample matrix.

In addition, we investigated two fjord water samples by solution MC-ICP-MS following the method as described in detail elsewhere.[47] Briefly, B was separated from matrix elements using the micro-distillation technique prior to analysis. An aliquot of 20 μL of seawater mixed with 20 μL of concentrated HNO_3 of ultrapure grade was distilled in Savillex Teflon fin-leg vials, which were placed upside down on a hotplate at 100°C for 24 h. The distillate contains only B in HNO_3, which was subsequently diluted with 0.3 M HNO_3 to obtain a solution with a B concentration of 100 ng g^{-1}. Boron isotopic ratios were measured in triplicate using Faraday cups equipped with resistors of 10^{11} Ω at the Nu Plasma II MC-ICP-MS. We employed the standard-sampling technique using NIST SRM 951 as bracketing standard.

All B isotopic data are reported in delta notation in permil units (‰) relative to NIST SRM 951. Data obtained by LA are recalculated relative to NIST SRM 951 by assuming a difference of −0.26‰ between the employed bracketing standard NIST SRM 610 and NIST SRM 951 as revealed by solution MC-ICP-MS[26]:

$$\delta^{11}B = \left(\frac{^{11}B/^{10}B_{Sample}}{^{11}B/^{10}B_{NIST\ SRM\ 951}} - 1 \right) \times 1000 \qquad (1)$$

3 | RESULTS

The carbonate material JCp-1 (powdered coral material *Porites* sp.) and the clay standard material IAEA-B-8 revealed average $\delta^{11}B$ values of 24.09 ± 0.87‰ (2 SD, $n = 17$) and −5.82 ± 0.67‰ (2 SD, $n = 11$), respectively. The selected reference materials of the MPI-DING glass series represent typical rock compositions and show average $\delta^{11}B$ values of −4.22 ± 0.54‰ (2 SD, $n = 3$) for ATHO-G (rhyolite), −4.24 ± 0.62‰ (2 SD, $n = 5$) for StHs6/80-G (andesite) and 8.34 ± 1.10‰ (2 SD, $n = 9$) for GOR132-G (komatiite). The silicate glass standard NIST SRM 612 is similar to NIST SRM 610 in matrix composition, but has lower trace element contents and an average $\delta^{11}B$ of −0.49 ± 0.65‰ (2 SD, $n = 14$). All obtained B isotopic values for reference materials (Table 1) are in the range of published values and show similar uncertainties independent of the sample matrix (Figure 3).

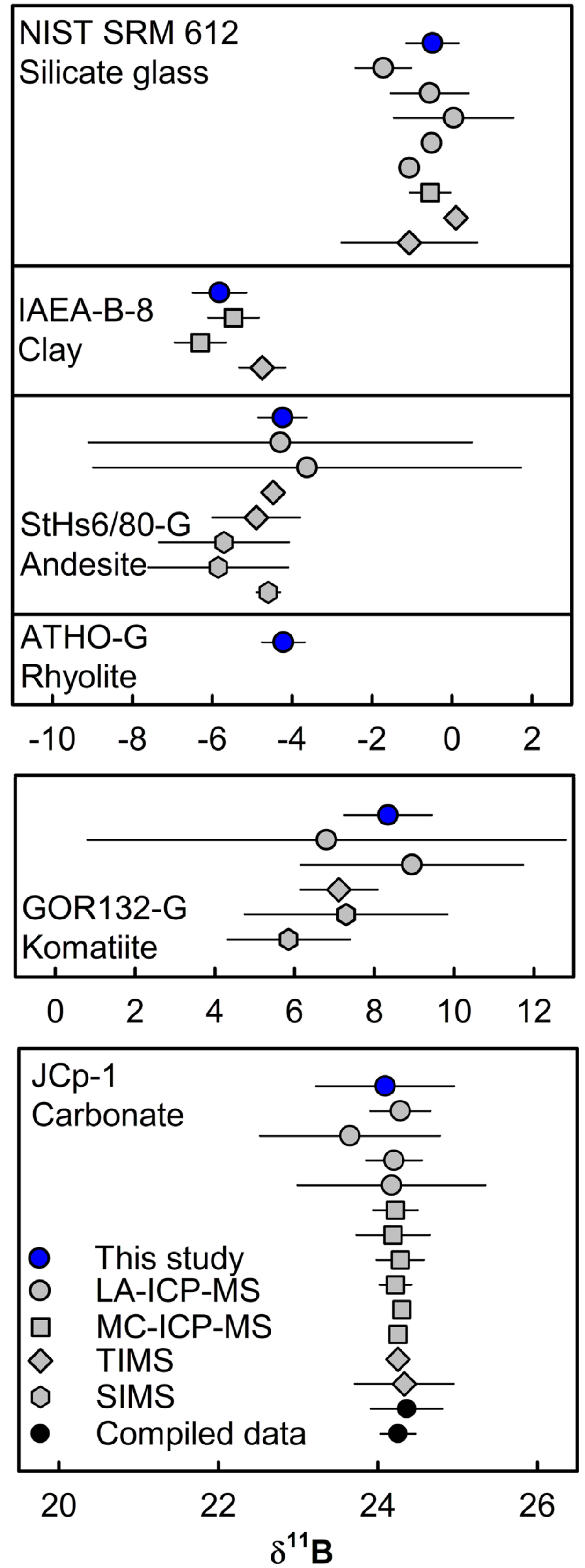

FIGURE 3 Legend on next page.

FIGURE 3 Boron isotopic data of reference materials. Error bars refer to ±2 SD, which are partly recalculated for literature data. In some cases, error bars are smaller than symbols representing the data. Depicted literature data are presented in the order from top to bottom as follows. For NIST SRM 612 (silicate glass): Kaczmarek et al[14] (recalculated relative to NIST SRM 951 assuming a difference of −0.26‰ between NIST SRM 951 and NIST SRM 610[26]), Fietzke et al,[13] Lin et al,[31] Kimura et al,[23] Fonseca et al,[59] Le Roux et al,[30] Jochum et al[60] and Kasemann et al[61]; for IAEA-B-8 (clay powder): Pi et al,[62] Cai et al[63] and Romer et al[64]; for StHs6/80-G (andesite glass): Tiepolo et al,[33] Lin et al,[31] Rosner and Meixner,[65] Jochum et al,[60] two data points from He et al[66] and Halama et al[67]; for GOR132-G (komatiite glass): Tiepolo et al,[33] Lin et al,[31] Rosner and Meixner,[65] two data points from He et al[66]; for JCp-1 (carbonate powder): Lloyd et al,[68] Standish et al,[26] Sadekov et al,[18] Fietzke and Wall,[10] Wang et al,[69] Chen et al,[70] Raitzsch et al,[47] Zhang et al,[71] Cai et al,[63] Lazareth et al,[72] Ishikawa and Nagaisgi[73] and Forster et al.[74] The black filled data points represent compiled data for JCp-1 from an interlaboratory study by Gutjahr et al[8] based on solution MC-ICP-MS and TIMS analyses: the upper black data point gives the average value for bulk sample material, the lower black data point represents the average value for sample material treated by an oxidative step to remove organic material. [Color figure can be viewed at wileyonlinelibrary.com]

We investigated several individual coral samples from field stations A (fjord head) and F (fjord mouth) in the Comau Fjord. Analyses of the coral sample from station A, BsCpI1-A, reveal an average $\delta^{11}B$ value of 25.83 ± 1.52‰ (2 SD, $n = 7$), whereas the samples from station F, CsCpI4-F and CsCpI9-F, give average $\delta^{11}B$ values of 23.35 ± 1.30‰ (2 SD, $n = 12$) (Figure 1) and 23.01 ± 2.21‰ (2 SD, $n = 10$), respectively (Table 4, Figure 4). A single analysis was conducted on a large septum of sample CsCpI4-F revealing a similar $\delta^{11}B$ value of 23.63‰. Individual coral samples show minor intra-skeleton variability in $\delta^{11}B$ as obtained uncertainties are higher compared to those revealed for reference materials. Investigated fjord water samples reveal $\delta^{11}B$ values of 40.37 ± 0.15‰ (2 SD, $n = 3$) for station A and 40.19 ± 0.37‰ (2 SD, $n = 3$) for station F, giving an average of 40.27‰ (Table 2).

TABLE 4 Boron isotopic data ($\delta^{11}B$) and calculated internal pH (pH_{cf}) values of investigated coral samples of *Desmophyllum dianthus*

Septa interspace	$\delta^{11}B$ (‰)	pH_{cf}
BsCpI1-A (fjord head; seawater $pH_T = 7.59$)		
6	27.38	8.82
7–1	26.25	8.75
7–2	25.61	8.71
7–3	25.53	8.71
8	24.82	8.66
9	25.28	8.69
11	25.94	8.73
Average	25.83 ± 1.52 (2 SD)	8.73 ± 0.05 (1 SD)
CsCpI9-F (fjord mouth; seawater $pH_T = 7.86$)		
1	22.08 (22.73; 21.43)	8.49
2	23.77	8.62
3	22.89 (23.64; 22.24)	8.55
4	20.78	8.40
5	22.19	8.50
6	23.04	8.56
7	25.08	8.69
8	23.56	8.59
9	23.76	8.60
10	22.98	8.55
Average	23.01 ± 2.21 (2 SD)	8.55 ± 0.08 (1 SD)
CsCpI4-F (fjord mouth; seawater $pH_T = 7.86$)		
1	22.90 (22.36; 23.44)	8.55
4	23.87 (23.03; 24.70)	8.61
5	23.37	8.58
6	22.33 (22.24; 22.33)	8.51
7	23.39	8.58
8–1	22.03 (22.35; 21.71)	8.49
8–2	23.62 (24.21; 23.02)	8.60
9–1	23.64 (23.37; 23.90)	8.63
9–2	24.15 (23.98; 24.33)	8.60
10	22.96	8.56
12–1	24.26	8.65
12–2	23.63	8.61
Average	23.35 ± 1.30 (2 SD)	8.58 ± 0.05 (1 SD)
Septum	23.63	8.59

Note: The average $\delta^{11}B$ value is provided for multiple analyses at the same spot with values of single measurements given in brackets.

4 | DISCUSSION

4.1 | Accurate and precise matrix-independent B isotope analysis

Several recent studies based on LA coupled to MC-ICP-MS report on the challenge of dealing with matrix effects,[12,18,26] whereas our study reveals accurate B isotopic ratios independently of the sample matrix. In this study, the obtained results of all investigated reference materials, including carbonate and various silicate matrices using the silicate glass NIST SRM 610 as bracketing standard, are highly consistent with published B isotopic data (Figure 3). These results demonstrate the capability of matrix-independent analysis of B isotopic ratios by this instrumental set-up, consisting of a UV fs LA system coupled to a Nu Plasma II MC-ICP-MS equipped with electron multiplier detectors. Neither laser-induced nor ICP-related matrix effects are detectable within the obtained precisions, independent of major differences in matrix composition and B concentration between the reference material and the bracketing standard. Contrarily, several other recent studies[12,16,18,26] disclosed considerable biases in $\delta^{11}B$ with respect to accepted values ranging from a few permils up to 20‰

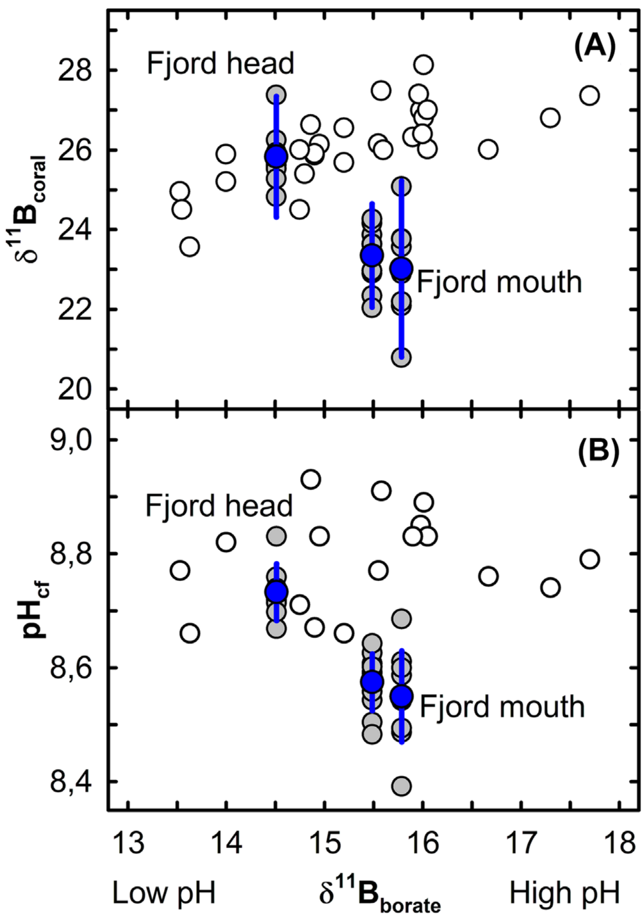

FIGURE 4 Boron isotopic data (A) and calculated internal pH values (pH_{cf}) (B) of investigated coral samples from the Comau Fjord (Chile) relative to B isotopic composition of seawater borate. Grey filled circles refer to individual data obtained at various interspaces for each investigated coral sample, whereas blue filled circles represent average data with error bars referring to 2 SD for $\delta^{11}B$ and 1 SD for pH_{cf}. Coral samples from the fjord mouth both grew under ambient seawater pH_T of 7.86, which corresponds to a $\delta^{11}B_{borate}$ value of 15.63‰, but are plotted slightly apart (offset 0.15‰) from each other for better visualization. Published data for *D. dianthus* are presented by open circles.[45,48–50] [Color figure can be viewed at wileyonlinelibrary.com]

for carbonates and silicates when using ns LA coupled to a Thermo Neptune Plus MC-ICP-MS equipped with Faraday cups with 10^{13} Ω resistors. These offsets are interpreted to result primarily from an unresolved interference caused by scattered Ca ions. However, there is also evidence that laser-induced fractionation at the ablation site contributes to observed offsets, especially for silicate matrices.[12] To obtain accurate $\delta^{11}B$ values, these authors developed a correction procedure based on an empirically determined logarithmic relationship between the offset to the accepted true value, $\Delta^{11}B$, and the B/Ca ratio for each sample matrix, which might require re-calibration during every analytical session. Nanosecond LA coupled to an AXIOM MC-ICP-MS does not show the effect of scattered ion but is sensitive to plasma conditions when analyzing carbonates.[10,24] The question arises as to why some instrumental set-ups produce offsets due to an unresolved interference of scattered Ca ions,[12,18,26] whereas others including this study reveal accurate results without applying correction modes.[11,13,30] This effect of scattered ions might be linked to the type of mass spectrometer in use and is likely related to the specific arrangement of ion optics, electrostatic analyzer, magnet and detector block in each instrument type. We can only speculate on possible causes as to why our analytical set-up is unaffected by this potential complication as more detailed investigations, and ideally cross-institutional collaborative efforts, would be required, which is beyond of the scope of this study. An obvious difference is the arrangement of the applied detectors. Studies conducted on a Thermo Neptune or Neptune Plus MC-ICP-MS employed Faraday cups, which detect ions after being dispersed according to their mass by the magnet.[12,18,26] In contrast, we applied electron multiplier detectors, which are located behind the Faraday collector block in a Nu Plasma II MC-ICP-MS. Additional installed ion optics steer ions through gaps between Faraday cups to electron multiplier detectors, which might contribute to minimize potential scattered ions of other elements. Beside the kind of mass spectrometer, the type of laser (ns versus fs pulses) might have an effect on matrix dependency, especially for silicates with a more complex matrix than carbonates. Although Evans et al[12] ascribed observed offsets in $\delta^{11}B$ for silicates mainly to scattered ions in the mass spectrometer, they also noted some laser-induced effects for their set-up (ns laser coupled to Thermo Neptune Plus), which are not observed for fs LA in this study. In conclusion, matrix effects seem mainly related to processes within the mass spectrometer, which are dependent on the type of instrument (no detectable effects for Nu Plasma II[11] (this study), scattered Ca ions for Thermo Neptune Plus,[12,18,26] plasma load effects for AXIOM MC-ICP-MS[10,24]), whereas the employment of a fs laser provides further improvement especially for samples with a complex matrix composition, that is, silicates[12] (this study).

Some LA-MC-ICP-MS studies using Faraday cups for detection achieved an external reproducibility of better than ±1‰ (2 SD) for silicate glasses.[12,23,29,30] In contrast, a more variable reproducibility has been reported for carbonate reference materials ranging between ±0.5‰ and 1.7‰ (2 SD).[12–14,18,26] In our study, we obtained a reproducibility of better than ±0.9‰ (2 SD) (slightly higher for GOR132-G) using electron multiplier detectors, independently of the sample matrix and type of sample preparation (pressed powder pellets versus glass beats) (Figure 3; Table 1). The same detector configuration of our mass spectrometer revealed a long-term reproducibility of ±0.3‰ (2 SD) for $\delta^{11}B$ using solution MC-ICP-MS for pure B standards, whereas multiple analyses of foraminifera samples subjected to chemical purification prior to analysis indicate a reproducibility of about ±0.6‰ (2 SD).[47] In comparison, analyses of B isotopic ratios by solution ICP-MS based on a Neptune/Neptune Plus MC-ICP-MS achieved a reproducibility of about ±0.2‰ (2 SD) using Faraday cups.[8] This demonstrates that our instrumental set-up, that is, a UV fs LA system coupled to a Nu Plasma II MC-ICP-MS, provides accurate and precise B isotopic data independently of the sample matrix with a reproducibility close to those obtained by solution MC-ICP-MS on the same mass spectrometer.

4.2 | Application to cold-water corals (*D. dianthus*)

4.2.1 | Spatial variability of B isotopic composition in coral samples

We investigated increments grown in austral spring in coral skeletons at interspaces between septa for each coral sample ($n = 7$ to 12) (Table 4) as shown for sample CsCpI4-F (Figure 1). Interestingly, the coral samples from the fjord mouth with a seawater pH_T of 7.86 reveal very similar average $\delta^{11}B$ values of 23.35 ± 1.30 (2 SD) and 23.01 ± 2.21 (2 SD), whereas the sample from the fjord head shows a higher average $\delta^{11}B$ value of 25.83 ± 1.52 (2 SD), despite a lower ambient seawater pH_T of 7.59 (Figure 4). However, the obtained average B isotopic compositions are in the range of published values for *D. dianthus* ($\delta^{11}B = 22.6‰$ to 28.1‰).[18,45,48–50] Individual samples show little intra-skeleton variation in $\delta^{11}B$ as reported reproducibility (2 SD) is close to those obtained for investigated reference materials. These minor variations might be related to microstructures as observed for the cold-water coral *Lophelia pertusa* (syn. *Desmophyllum pertusum*),[10] the tropical coral *Siderastrea siderea*[46] and also for *D. dianthus* in the Comau Fjord, which is more pronounced than for species grown under more steady open-ocean conditions.[45] Overall, the B isotopic data suggest that B incorporation into coral skeletons during calcification is a relatively uniform process in each individual coral over the considered growth period (austral spring). The similarity in $\delta^{11}B$ of the investigated coral samples from the fjord mouth suggests that the calcification process is also consistent on a seasonal scale across individual corals grown under the same environmental conditions. Contrary to expectations, the coral sample from the fjord head shows a higher $\delta^{11}B$ value than those at the fjord mouth suggesting that also other parameters beside seawater pH_T affect the B isotopic record of corals from the Comau Fjord (see discussion below).

4.2.2 | Boron isotopic composition translated into internal pH of cold-water corals

Scleractinian corals have the capability to up-regulate their internal pH in the calcifying fluid with respect to seawater to promote calcification.[51] This mechanism enables corals to adapt to low-pH environments, providing some resilience to ocean acidification.[52,53] Measured $\delta^{11}B$ values in coral skeletons can be converted into the pH of the internal calcifying fluid (pH_{cf}) using the following equation[51]:

$$pH_{cf} = pK_B - \log\left[\frac{\delta^{11}B_{SW} - \delta^{11}B_{carb}}{\alpha \times \delta^{11}B_{coral} - \delta^{11}B_{SW} + 1000 \times (\alpha - 1)}\right] \quad (2)$$

where $\delta^{11}B_{SW}$ is the isotopic composition of ambient seawater, $\delta^{11}B_{coral}$ is the average isotopic composition of the coral sample, the isotopic fractionation factor α between boric acid and borate is 1.0272,[54] and pK_B refers to the dissociation constant. The dissociation constant of boric acid pK_B[55] is calculated by the Seacarb package[56] in the software R[57] using salinity and temperature data giving a value of 8.763 (Table 1). Typically, B isotopic data of biogenic carbonates are depicted relative to B isotopic composition of seawater borate $\delta^{11}B_{borate}$ calculated from carbonate chemistry data (Figure 4), which relates to seawater pH_T by the following equation:

$$\delta^{11}B_{borate} = \frac{\delta^{11}B_{SW} + \left[\delta^{11}B_{SW} - 1000 \times (\alpha - 1)\right] \times 10^{pK_B - pH_T}}{1 + \alpha \times 10^{pK_B - pH_T}} \quad (3)$$

The difference between pH_{cf} and ambient seawater pH_T describes the biological induced up-regulation ΔpH as follows:

$$\Delta pH = pH_{cf} - pH_T \quad (4)$$

The two coral samples from the fjord mouth, CsCpI4-F and CsCpI9-F, reveal almost identical pH_{cf} values of 8.58 ± 0.05 (1 SD) and 8.55 ± 0.08 (1 SD), respectively, which correspond to an up-regulation of 0.7 pH units (Table 4, Figure 4). Although the seawater pH_T is lower at the fjord head, the investigated sample indicates enhanced pH up-regulation of 1.1 pH units, reaching a higher pH_{cf} value of 8.73 ± 0.05 (1 SD) compared to those from the fjord mouth (Table 4, Figure 4). The revealed up-regulation is within the range detected in the calcifying fluid of several cold-water coral species, showing an increase of about 0.6 to 1.3 pH units relative to seawater pH_T.[48,49,52,53,58] However, studies on the capability of pH up-regulation of cold-water corals have revealed opposing results, suggesting that also other environmental parameters beside seawater pH_T may influence up-regulation (see also Table 2). Previous investigations on *D. dianthus* revealed a correlation between low $\delta^{11}B$ values and low seawater pH_T values, which implies that physiological pH up-regulation can only partly compensate for low ambient seawater pH_T.[45,48,49] In contrast, a study on the closely related, but colony-forming, cold-water coral species *L. pertusa* found little variability in B isotopic composition independently of seawater conditions, which suggests that corals have the potential to compensate for acidified conditions, likely due to enough food resources.[53] Likewise, a recent study showed that the high abundance of zooplankton enhances the growth of cold-water corals in the Comau Fjord even in shallow depth.[40] Beside distinct fjord conditions, potential small-scale variability in $\delta^{11}B$ related to microstructures in the skeletons[10,45] and a rather poor control on pH conditions in a highly dynamic fjord system might obscure a correlation between seawater pH_T and $\delta^{11}B$ as revealed for *D. dianthus* from open-ocean conditions (Figure 4).[45,48–50]

5 | CONCLUSION

This study demonstrates that UV fs LA coupled to MC-ICP-MS (Nu Plasma II) provides a unique *in situ* technique to obtain accurate and precise B isotopic data, independently of the sample matrix using the glass NIST SRM 610 as calibration standard. Multiple analyses of silicate and carbonate reference materials reveal average $\delta^{11}B$ values, which are identical within analytical uncertainties to published data obtained by solution MC-ICP-MS or TIMS. We obtained an external reproducibility of ±0.9‰ (2 SD) independent of the sample matrix by consuming sample material with an equivalent amount of less than 0.1 ng of B. Application to cold-water corals (*D. dianthus*) from a field experiment in the Chilean Comau Fjord reveals average $\delta^{11}B$ values ranging between 23.01‰ and 25.83‰ for skeleton increments grown during austral spring with minor intra-skeleton variability. Inferred internal pH values of calcifying fluids reveal an up-regulation of 0.7 to 1.1 pH units relative to ambient seawater pH_T. This approach opens a wide field of application, including pH reconstruction in biogenic carbonates and deciphering processes related to fluid–mineral interaction in low- and high-temperature geochemistry.

ACKNOWLEDGMENTS

The authors appreciate the analytical support by Ingo Horn and by the staff of the AWI ICP facility. Klaus Peter Jochum provided pieces of investigated MPI-DING glasses. The field expedition teams and the staff of the Huinay scientific field station are thanked for excavating coral samples from the Comau Fjord by SCUBA diving in September 2016 and January 2017. We appreciate the editorial handling by R. Bol and the constructive comments by T. Chalk and J. Stewart, which improved the manuscript. Export permits for *D. dianthus* according to the Convention on International Trade in Endangered Species of Wild Fauna and Flora (CITES) were admitted by the Chilean Servicio Nacional de Pesca y Acuicultura (Sernapesca; Permiso CITES No. 17000003WS) and import permits by the German Federal Agency for Nature Conservation (BfN; E00134/17 and E00430/17). This study was supported by the bilateral Chilean–German project PACOC (CONICYT-BMBF (Bundesministerium für Bildung und Forschung): 20140041 and 01DN15024, CONICYT FONDAP-IDEAL 15150003) and by the project DACCOR funded by the AWI Strategy Fund and contributes to the Helmholtz Research Program *Changing Earth – Sustaining our Future*: Subtopics 2.4., 2.1, 4.1 and 6.1 at AWI. Open Access funding enabled and organized by Projekt DEAL.

DATA AVAILABILITY STATEMENT

The data that supports the findings of this study are available in this article or have been published before.

ORCID

Grit Steinhoefel https://orcid.org/0000-0001-7802-1619

PEER REVIEW

The peer review history for this article is available at https://www.webofscience.com/api/gateway/wos/peer-review/10.1002/rcm.9508.

REFERENCES

1. Marschall H, Foster G. *Boron Isotopes – The Fifth Element*. Springer International Publishing AG; 2018. doi:10.1007/978-3-319-64666-4
2. Anagnostou E, John EH, Edgar KM, et al. Changing atmospheric CO_2 concentration was the primary driver of early Cenozoic climate. *Nature*. 2016;533(7603):380-384. doi:10.1038/nature17423
3. Fietzke J, Ragazzola F, Halfar J, et al. Century-scale trends and seasonality in pH and temperature for shallow zones of the Bering Sea. *Proc Natl Acad Sci USA*. 2015;112(10):2960-2965. doi:10.1073/pnas.1419216112
4. Foster GL. Seawater pH, pCO_2 and $[CO_3^{2-}]$ variations in the Caribbean Sea over the last 130 kyr: A boron isotope and B/Ca study of planktic forminifera. *Earth Planet Sci Lett*. 2008;271(1-4):254-266. doi:10.1016/j.epsl.2008.04.015
5. Hoenisch B, Hemming NG, Archer D, Siddall M, McManus JF. Atmospheric carbon dioxide concentration across the mid-Pleistocene transition. *Science*. 2009;324(5934):1551-1554. doi:10.1126/science.1171477
6. Jurikova H, Liebetrau V, Raddatz J, et al. Boron isotope composition of the cold-water coral *Lophelia pertusa* along the Norwegian margin: Zooming into a potential pH-proxy by combining bulk and high-resolution approaches. *Chem Geol*. 2019;513:143-152. doi:10.1016/j.chemgeo.2019.01.005
7. Rae JWB, Sarnthein M, Foster GL, Ridgwell A, Grootes PM, Elliott T. Deep water formation in the North Pacific and deglacial CO_2 rise. *Paleoceanography*. 2014;29(6):645-667. doi:10.1002/2013PA002570
8. Gutjahr M, Bordier L, Douville E, et al. Sub-permil interlaboratory consistency for solution-based boron isotope analyses on marine carbonates. *Geostand Geoanal Res*. 2021;45(1):59-75. doi:10.1111/ggr.12364
9. Stewart JA, Christopher SJ, Kucklick JR, et al. NIST RM 8301 boron isotopes in marine carbonate (simulated coral and foraminifera solutions): Inter-laboratory $\delta^{11}B$ and trace element ratio value assignment. *Geostand Geoanal Res*. 2021;45(1):77-96. doi:10.1111/ggr.12363
10. Fietzke J, Wall M. Distinct fine-scale variations in calcification control revealed by high-resolution 2D boron laser images in the cold-water coral *Lophelia pertusa*. *Sci Adv*. 2022;8(11):eabj4172.
11. Raitzsch M, Rollion-Bard C, Horn I, et al. Single-shell $\delta^{11}B$ analysis of *Cibicidoides wuellerstorfi* using femtosecond laser ablation MC-ICP-MS and secondary ion mass spectrometry. *Biogeosciences*. 2020;17(21):5365-5375. doi:10.5194/bg-17-5365-2020
12. Evans D, Gerdes A, Coenen D, Marschall HR, Müller W. Accurate correction for the matrix interference on laser ablation MC-ICP-MS boron isotope measurements in $CaCO_3$ and silicate matrices. *J Anal At Spectrom*. 2021;36(8):1607-1617. doi:10.1039/D1JA00073J
13. Fietzke J, Heinemann A, Taubner I, Boehm F, Erez J, Eisenhauer A. Boron isotope ratio determination in carbonates via LA-MC-ICP-MS using soda-lime glass standards as reference material. *J Anal At Spectrom*. 2010;25(12):1953-1957. doi:10.1039/c0ja00036a
14. Kaczmarek K, Horn I, Nehrke G, Bijma J. Simultaneous determination of delta B-11 and B/Ca ratio in marine biogenic carbonates at nanogram level. *Chem Geol*. 2015;392:32-42. doi:10.1016/j.chemgeo.2014.11.011
15. Kasemann SA, Schmidt DN, Bijma J, Foster GL. In situ boron isotope analysis in marine carbonates and its application for foraminifera and palaeo-pH. *Chem Geol*. 2009;260(1-2):138-147. doi:10.1016/j.chemgeo.2008.12.015
16. Míková J, Košler J, Wiedenbeck M. Matrix effects during laser ablation MC-ICP-MS analysis of boron isotopes in tourmaline. *J Anal At Spectrom*. 2014;29(5):903-914. doi:10.1039/c3ja50241d
17. Rollion-Bard C, Chaussidon M, France-Lanord C. Biological control of internal pH in scleractinian corals: Implications on paleo-pH and paleo-temperature reconstructions. *C R Geosci*. 2011;343(6):397-405. doi:10.1016/j.crte.2011.05.003
18. Sadekov A, Lloyd NS, Misra S, Trotter J, D'Olivo J, McCulloch M. Accurate and precise microscale measurements of boron isotope ratios in calcium carbonates using laser ablation multicollector-ICPMS. *J Anal At Spectrom*. 2019;34(3):550-560. doi:10.1039/c8ja00444g

19. Fernández B, Claverie F, Pécheyran C, Donard OF. Direct analysis of solid samples by fs-LA-ICP-MS. *TrAC Trends Anal Chem*. 2007;26(10): 951-966. doi:10.1016/j.trac.2007.08.008
20. Garcia CC, Lindner H, Niemax K. Laser ablation inductively coupled plasma mass spectrometry – Current shortcomings, practical suggestions for improving performance, and experiments to guide future development. *J Anal At Spectrom*. 2009;24(1):14-26. doi:10.1039/B813124B
21. Horn I, von Blanckenburg F. Investigation on elemental and isotopic fractionation during 196 nm femtosecond laser ablation multiple collector inductively coupled plasma mass spectrometry. *Spectrochim Acta B*. 2007;62(4):410-422. doi:10.1016/j.sab.2007.03.034
22. Jochum KP, Stoll B, Weis U, Jacob DE, Mertz-Kraus R, Andreae MO. Non-matrix-matched calibration for the multi-element analysis of geological and environmental samples using 200 nm femtosecond LA-ICP-MS: A comparison with nanosecond lasers. *Geostand Geoanal Res*. 2014;38(3):265-292. doi:10.1111/j.1751-908X.2014.12028.x
23. Kimura JI, Chang Q, Ishikawa T, Tsujimori T. Influence of laser parameters on isotope fractionation and optimisation of lithium and boron isotope ratio measurements using laser ablation-multiple Faraday collector-inductively coupled plasma mass spectrometry. *J Anal At Spectrom*. 2016;31(11):2305-2320. doi:10.1039/c6ja00283h
24. Fietzke J, Frische M. Experimental evaluation of elemental behavior during LA-ICP-MS: Influences of plasma conditions and limits of plasma robustness. *J Anal At Spectrom*. 2016;31(1):234-244. doi:10.1039/c5ja00253b
25. Dishon G, Fisch J, Horn I, et al. A novel paleo-bleaching proxy using boron isotopes and high-resolution laser ablation to reconstruct coral bleaching events. *Biosciences*. 2015;12(19):5677-5687. doi:10.5194/bg-12-5677-2015
26. Standish CD, Chalk TB, Babila TL, Milton JA, Palmer MR, Foster GL. The effect of matrix interferences on in situ boron isotope analysis by laser ablation multi-collector inductively coupled plasma mass spectrometry. *Rapid Commun Mass Spectrom*. 2019;33(10):959-968. doi:10.1002/rcm.8432
27. Thil F, Blamart D, Assailly C, et al. Development of laser ablation multi-collector inductively coupled plasma mass spectrometry for boron isotopic measurement in marine biocarbonates: New improvements and application to a modern Porites coral. *Rapid Commun Mass Spectrom*. 2016;30(3):359-371. doi:10.1002/rcm.7448
28. Cheng L, Zhang C, Liu X, et al. Significant boron isotopic fractionation in the magmatic evolution of Himalayan leucogranite recorded in multiple generations of tourmaline. *Chem Geol*. 2021;571:120194. doi:10.1016/j.chemgeo.2021.120194
29. Devulder V, Gerdes A, Vanhaecke F, Degryse P. Validation of the determination of the B isotopic composition in Roman glasses with laser ablation multi-collector inductively coupled plasma-mass spectrometry. *Spectrochim Acta B*. 2015;105(SI):116-120. doi:10.1016/j.sab.2014.08.038
30. le Roux P, Shirey S, Benton L, Hauri E, Mock T. In situ, multiple-multiplier, laser ablation ICP-MS measurement of boron isotopic composition (delta B-11) at the nanogram level. *Chem Geol*. 2004; 203(1-2):123-138. doi:10.1016/j.chemgeo.2003.09.006
31. Lin L, Hu Z, Yang L, et al. Determination of boron isotope compositions of geological materials by laser ablation MC-ICP-MS using newly designed high sensitivity skimmer and sample cones. *Chem Geol*. 2014;386:22-30. doi:10.1016/j.chemgeo.2014.08.001
32. Martin C, Ponzevera E, Harlow G. In situ lithium and boron isotope determinations in mica, pyroxene, and serpentine by LA-MC-ICP-MS. *Chem Geol*. 2015;412:107-116. doi:10.1016/j.chemgeo.2015.07.022
33. Tiepolo M, Bouman C, Vannucci R, Schwieters J. Laser ablation multicollector ICPMS determination of delta B-11 in geological samples. *Appl Geochem*. 2006;21(5):788-801. doi:10.1016/j.apgeochem.2006.02.014
34. Steinhoefel G, Breuer J, von Blanckenburg F, Horn I, Sommer M. The dynamics of Si cycling during weathering in two small catchments in the Black Forest (Germany) traced by Si isotopes. *Chem Geol*. 2017;466:389-402. doi:10.1016/j.chemgeo.2017.06.026
35. Steinhoefel G, Breuer J, von Blanckenburg F, Horn I, Kaczorek D, Sommer M. Micrometer silicon isotope diagnostics of soils by UV femtosecond laser ablation. *Chem Geol*. 2011;286(3-4):280-289. doi:10.1016/j.chemgeo.2011.05.013
36. Jochum KP, Nohl U, Herwig K, Lammel E, Stoll B, Hofmann AW. GeoReM: A new geochemical database for reference materials and isotopic standards. *Geostand Geoanal Res*. 2005;29(3):333-338. doi:10.1111/j.1751-908X.2005.tb00904.x
37. Beck KK, Schmidt-Grieb GM, Laudien J, et al. Environmental stability and phenotypic plasticity benefit the cold-water coral *Desmophyllum dianthus* in an acidified fjord. *Commun Biol*. 2022;5(1):683. doi:10.1038/s42003-022-03622-3
38. Fillinger L, Richter C. Vertical and horizontal distribution of *Desmophyllum dianthus* in Comau Fjord, Chile: A cold-water coral thriving at low pH. *PeerJ*. 2013;1:e194. doi:10.7717/peerj.194
39. Rossbach S, Rossbach FI, Häussermann V, Försterra G, Laudien J. In situ skeletal growth rates of the solitary cold-water coral *Tethocyathus endesa* from the Chilean fjord region. *Front Mar Sci*. 2021;8:757702.
40. Garcia-Herrera N, Cornils A, Laudien J, et al. Seasonal and diel variations in the vertical distribution, composition, abundance and biomass of zooplankton in a deep Chilean Patagonian fjord. *PeerJ*. 2022;10:e12823. doi:10.7717/peerj.12823
41. Pierrot D, Lewis, E, Wallace DR. MS Excel program developed for CO_2 system calculations. ORNL Environmental Sciences Division. 2006.
42. Richter S, Konegger-Kappel S, Boulyga SF, Stadelmann G, Koepf A, Siegmund H. Linearity testing and dead-time determination for MC-ICP-MS ion counters using the IRMM-072 series of uranium isotope reference materials. *J Anal At Spectrom*. 2016;31(8): 1647-1657. doi:10.1039/C6JA00203J
43. Davis DW. A simple method for rapid calibration of Faraday and ion-counting detectors on movable multicollector mass spectrometers. *J Mass Spectrom*. 2020;55(6):e4511. doi:10.1002/jms.4511
44. Robinson LF, Adkins JF, Frank N, et al. The geochemistry of deep-sea coral skeletons: A review of vital effects and applications for palaeoceanography. *Deep-Sea Res II Top Stud Oceanogr*. 2014;99:184-198. doi:10.1016/j.dsr2.2013.06.005
45. Stewart JA, Anagnostou E, Foster GL. An improved boron isotope pH proxy calibration for the deep-sea coral *Desmophyllum dianthus* through sub-sampling of fibrous aragonite. *Chem Geol*. 2016;447: 148-160. doi:10.1016/j.chemgeo.2016.10.029
46. Chalk TB, Standish CD, D'Angelo C, Castillo KD, Milton JA, Foster GL. Mapping coral calcification strategies from in situ boron isotope and trace element measurements of the tropical coral *Siderastrea siderea*. *Sci Rep*. 2021;11(1):1-13. doi:10.1038/s41598-020-78778-1
47. Raitzsch M, Bijma J, Benthien A, Richter KU, Steinhoefel G, Kučera M. Boron isotope-based seasonal paleo-pH reconstruction for the Southeast Atlantic – A multispecies approach using habitat preference of planktonic foraminifera. *Earth Planet Sci Lett*. 2018;487: 138-150. doi:10.1016/j.epsl.2018.02.002
48. Anagnostou E, Huang KF, You CF, Sikes EL, Sherrell RM. Evaluation of boron isotope ratio as a pH proxy in the deep sea coral *Desmophyllum dianthus*: Evidence of physiological pH adjustment. *Earth Planet Sci Lett*. 2012;349:251-260. doi:10.1016/j.epsl.2012.07.006
49. McCulloch M, Trotter J, Montagna P, et al. Resilience of cold-water scleractinian corals to ocean acidification: Boron isotopic systematics of pH and saturation state up-regulation. *Geochim Cosmochim Acta*. 2012;87:21-34. doi:10.1016/j.gca.2012.03.027

50. Rae JW, Burke A, Robinson LF, et al. CO_2 storage and release in the deep Southern Ocean on millennial to centennial timescales. *Nature*. 2018;562(7728):569-573. doi:10.1038/s41586-018-0614-0
51. McCulloch MT, D'Olivo JP, Falter J, et al. Boron isotopic systematics in scleractinian corals and the role of pH up-regulation. In: *Boron Isotopes*. Springer; 2018:145-162.
52. Prouty NG, Wall M, Fietzke J, et al. The role of pH up-regulation in response to nutrient-enriched, low-pH groundwater discharge. *Mar Chem*. 2022;243:104134. doi:10.1016/j.marchem.2022.104134
53. Wall M, Ragazzola F, Foster LC, Form A, Schmidt DN. pH up-regulation as a potential mechanism for the cold-water coral *Lophelia pertusa* to sustain growth in aragonite undersaturated conditions. *Biogeosciences*. 2015;12(23):6869-6880. doi:10.5194/bg-12-6869-2015
54. Klochko K, Kaufman AJ, Yao W, Byrne RH, Tossell JA. Experimental measurement of boron isotope fractionation in seawater. *Earth Planet Sci Lett*. 2006;248(1-2):276-285. doi:10.1016/j.epsl.2006.05.034
55. Dickson AG. Thermodynamics of the dissociation of boric acid in synthetic seawater from 273.15 to 318.15 K. *Deep Sea Res A Oceanogr Res Pap*. 1990;37(5):755-766. doi:10.1016/0198-0149(90)90004-F
56. Gattuso JP, Epitalon JM, Lavigne H, Orr J. seacarb: Seawater carbonate chemistry. R package version 3.2. 12. Published online 2019.
57. R Core Team. *R: A Language and Environment for Statistical Computing*. R Foundation for Statistical Computing; 2021.
58. Blamart D, Rollion-Bard C, Meibom A, Cuif JP, Juillet-Leclerc A, Dauphin Y. Correlation of boron isotopic composition with ultrastructure in the deep-sea coral *Lophelia pertusa*: Implications for biomineralization and paleo-pH. *Geochem Geophys Geosyst*. 2007;8(12):2007GC001686. doi:10.1029/2007GC001686
59. Fonseca RO, Kirchenbaur M, Ballhaus C, et al. Fingerprinting fluid sources in Troodos ophiolite complex orbicular glasses using high spatial resolution isotope and trace element geochemistry. *Geochim Cosmochim Acta*. 2017;200:145-166. doi:10.1016/j.gca.2016.12.012
60. Jochum KP, Wilson SA, Abouchami W, et al. GSD-1G and MPI-DING reference glasses for in situ and bulk isotopic determination. *Geostand Geoanal Res*. 2011;35(2):193-226. doi:10.1111/j.1751-908X.2010.00114.x
61. Kasemann S, Meixner A, Rocholl A, et al. Boron and oxygen isotope composition of certified reference materials NIST SRM 610/612 and reference materials JB-2 and JR-2. *Geostandards Newsletter*. 2001;25(2-3):405-416. doi:10.1111/j.1751-908X.2001.tb00615.x
62. Pi JL, You CF, Chung CH. Micro-sublimation separation of boron in rock samples for isotopic measurement by MC-ICPMS. *J Anal At Spectrom*. 2014;29(5):861-867. doi:10.1039/C3JA50344E
63. Cai Y, Rasbury ET, Wooton KM, Jiang X, Wang D. Rapid boron isotope and concentration measurements of silicate geological reference materials dissolved through sodium peroxide sintering. *J Anal At Spectrom*. 2021;36(10):2153-2163. doi:10.1039/D1JA00195G
64. Romer RL, Meixner A, Hahne K. Lithium and boron isotopic composition of sedimentary rocks – The role of source history and depositional environment: A 250 Ma record from the Cadomian orogeny to the Variscan orogeny. *Gondw Res*. 2014;26(3-4):1093-1110. doi:10.1016/j.gr.2013.08.015
65. Rosner M, Meixner A. Boron isotopic composition and concentration of ten geological reference materials. *Geostand Geoanal Res*. 2004;28(3):431-441. doi:10.1111/j.1751-908X.2004.tb00761.x
66. He M, Xia X, Huang X, et al. Rapid determination of the original boron isotopic composition from altered basaltic glass by in situ secondary ion mass spectrometry. *J Anal At Spectrom*. 2020;35(2):238-245. doi:10.1039/c9ja00374f
67. Halama R, Konrad-Schmolke M, De Hoog J. Boron isotope record of peak metamorphic ultrahigh-pressure and retrograde fluid–rock interaction in white mica (Lago di Cignana, Western Alps). *Contrib Mineral Petrol*. 2020;175(3):20. doi:10.1007/s00410-020-1661-8
68. Lloyd NS, Sadekov AY, Misra S. Application of 1013 ohm Faraday cup current amplifiers for boron isotopic analyses by solution mode and laser ablation multicollector inductively coupled plasma mass spectrometry. *Rapid Commun Mass Spectrom*. 2018;32(1):9-18. doi:10.1002/rcm.8009
69. Wang BS, You CF, Huang KF, et al. Direct separation of boron from Na- and Ca-rich matrices by sublimation for stable isotope measurement by MC-ICP-MS. *Talanta*. 2010;82(4):1378-1384. doi:10.1016/j.talanta.2010.07.010
70. Chen X, Deng W, Zhu H, Zhang Z, Wei G, McCulloch MT. Assessment of coral $\delta^{44/40}Ca$ as a paleoclimate proxy in the Great Barrier Reef of Australia. *Chem Geol*. 2016;435:71-78. doi:10.1016/j.chemgeo.2016.04.024
71. Zhang S, Henehan MJ, Hull PM, et al. Investigating controls on boron isotope ratios in shallow marine carbonates. *Earth Planet Sci Lett*. 2017;458:380-393. doi:10.1016/j.epsl.2016.10.059
72. Lazareth CE, Soares-Pereira C, Douville E, et al. Intra-skeletal calcite in a live-collected *Porites* sp.: Impact on environmental proxies and potential formation process. *Geochim Cosmochim Acta*. 2016;176:279-294. doi:10.1016/j.gca.2015.12.020
73. Ishikawa T, Nagaishi K. High-precision isotopic analysis of boron by positive thermal ionization mass spectrometry with sample preheating. *J Anal At Spectrom*. 2011;26(2):359-365. doi:10.1039/C0JA00060D
74. Foster GL, Hoenisch B, Paris G, et al. Interlaboratory comparison of boron isotope analyses of boric acid, seawater and marine $CaCO_3$ by MC-ICP-MS and NTIMS. *Chem Geol*. 2013;358:1-14. doi:10.1016/j.chemgeo.2013.08.027

How to cite this article: Steinhoefel G, Beck KK, Benthien A, Richter K-U, Schmidt-Grieb GM, Bijma J. Matrix-independent boron isotope analysis of silicate and carbonate reference materials by ultraviolet femtosecond laser ablation multi-collector inductively coupled plasma mass spectrometry with application to the cold-water coral *Desmophyllum dianthus*. *Rapid Commun Mass Spectrom*. 2023;37(13):e9508. doi:10.1002/rcm.9508